Jurnal Ilmu dan Teknologi Kelautan Tropis

p-ISSN: 2087-9423
e-ISSN: 2620-309X

Mechanisms of Vertical Mixing Over the Shelf Region in the Southwestern Arafura Sea

Muhammad Raafi[a], Yuli Naulita[b], I Wayan Nurjaya[b], Rastina[b]

[a] Graduate School in Marine Science, Faculty of Fisheries and Marine Sciences, IPB University, Darmaga Campus, Bogor 16680, Indonesia

[b] Department of Marine Science and Technology, Faculty of Fishery and Marine Science, IPB University, Darmaga Campus, Bogor 16680, Indonesia

Article Info:
Received 16 December 2025
Revised 17 March 2026
Accepted 07 April 2026

Corresponding Author:
Yuli Naulita
Department of Marine Science and Technology
IPB University
E-mail: naulita@apps.ipb.ac.id

Abstract

Vertical mixing regulates nutrient supply and productivity in surface layer, yet the controlling mechanisms remain unclear. Over shelf regions such as the southwestern Arafura Sea, steep topography and strong semidiurnal tides suggest that internal tide topography interactions may enhance turbulence. Unfortunately, observational links among stratification, topographically driven mixing processes, and internal tides remain limited in this region. This study investigates the dominant mechanisms controlling vertical mixing over the shelf region using hydrographic profiles, indirect turbulent measurements, and internal-tide diagnostics. We examined the stability, water masses, and turbulent kinetic energy dissipation rate (ε) and vertical eddy diffusivity ($K\rho$) from Thorpe-scale overturns. Internal-tide influence was assessed through M_2 ray path modeling and by sampling the M_2 tidal envelope at CTD cast times. Results show that the 50-200 m thermocline forms a barrier that suppresses mixing offshore and on the shelf, where $K\rho$ generally remains below 10^{-4} m^2 s^{-1}. Along the slope, weaker stratification at 600-1,000 m supports large overturns and elevated ε (10^{-7}-10^{-8} W kg^{-1}). Ri# indicates weak background shear, while Tu identifies salt-finger–favorable conditions contributing to mid-depth mixing. The spatial alignment between elevated ε and the shifted M_2 envelope, consistent with M_2 ray path geometry, suggests that internal tides reflected from locally supercritical topography enhance turbulence at the slope. These findings highlight the slope as a focused mixing hotspot. Future work should use moored velocity and high-resolution models to better resolve internal-tide energy pathways and their biogeochemical impacts.

Keywords: Arafura Sea, Internal Tide, Shelf Region, Vertical Mixing

1. Introduction

The Arafura Sea is part of the Indonesian Seas, connected to the Coral Sea through the Torres Strait in the east, and to the Banda and Timor Seas through the continental shelf and slope near Yamdena Island in the west. As a highly productive marine region (>300 g C m^{-2} yr^{-1}), its ecosystem is supported by the supply of nutrient-rich waters originating from the Banda Sea during the southeast monsoon (Kämpf, 2015). Previous studies show that enhanced turbulent kinetic energy dissipation rate and vertical eddy diffusivity can accelerate the upward transport of nutrients and subsequently stimulate phytoplankton production (Kobari et al., 2020; Tsutsumi et al., 2020; Yang et al., 2020; Acabado et al., 2021; Estrada-Allis et al., 2023). However, despite its ecological importance, the physical mechanisms that generate intense turbulent mixing in the southwestern Arafura Sea, particularly the interaction between internal tides and topography near Yamdena Island remain poorly understood.

One mechanism that can influence mixing in this region is internal tides. Strong tidal currents interacting with steep topography generate internal waves that propagate into deeper waters. When these waves reflect or break, their energy is converted into turbulence, causing vertical mixing and the upward movement of colder and nutrient-rich water (Mackinnon et al., 2013; Nugroho et al., 2018). Previous studies also indicate that Indonesian Seas are characterized by energetic internal tides, as shown by various two-dimensional and three-dimensional numerical simulations (Capuano et al., 2022). Although this mechanism has been documented in other parts of the Indonesian archipelago, its

influence in the southwestern Arafura Sea, particularly near the Yamdena region, has not been clearly described.

Based on these considerations, we hypothesize that the interaction between strong tidal currents and steep topography near the Yamdena continental slope generates energetic internal tides that act as a dominant driver of turbulent mixing in the southwestern Arafura Sea. This process is expected to enhance vertical shear and instability within the water column, thereby increasing turbulent kinetic energy (TKE) dissipation rate and vertical eddy diffusivity.

Therefore, this study investigates the mechanisms that control vertical mixing over the shelf region in the southwestern Arafura Sea by combining water-column stratification analysis with hydrodynamic indicators of instability: the Richardson Number (*Ri#*), Turner angle (*Tu*), and internal-tide ray path modeling (M_2). By integrating turbulence estimates derived from Thorpe-scale overturns (ε, $K\rho$) with these diagnostics, this study aims to identify where and why mixing hotspots develop, and to clarify the relative importance of shear instability, double diffusion, and internal tide breaking along the continental slope.

2. Materials and Methods

2.1. Materials

Fourteen CTD (Conductivity, Temperature, Depth) casts were carried out across the shelf in the southwestern Arafura Sea in February 2020. The spatial distribution of the CTD stations and the study area are shown in **Figure 1**, which presents the location map of the southwestern Arafura Sea near Yamdena Island. The CTD is Sea-Bird SBE 19Plus V2 CTD with sampling frequency 2 Hz. In addition to estimating turbulent mixing, the CTD data also served as the primary reference for validating the reanalysis data.

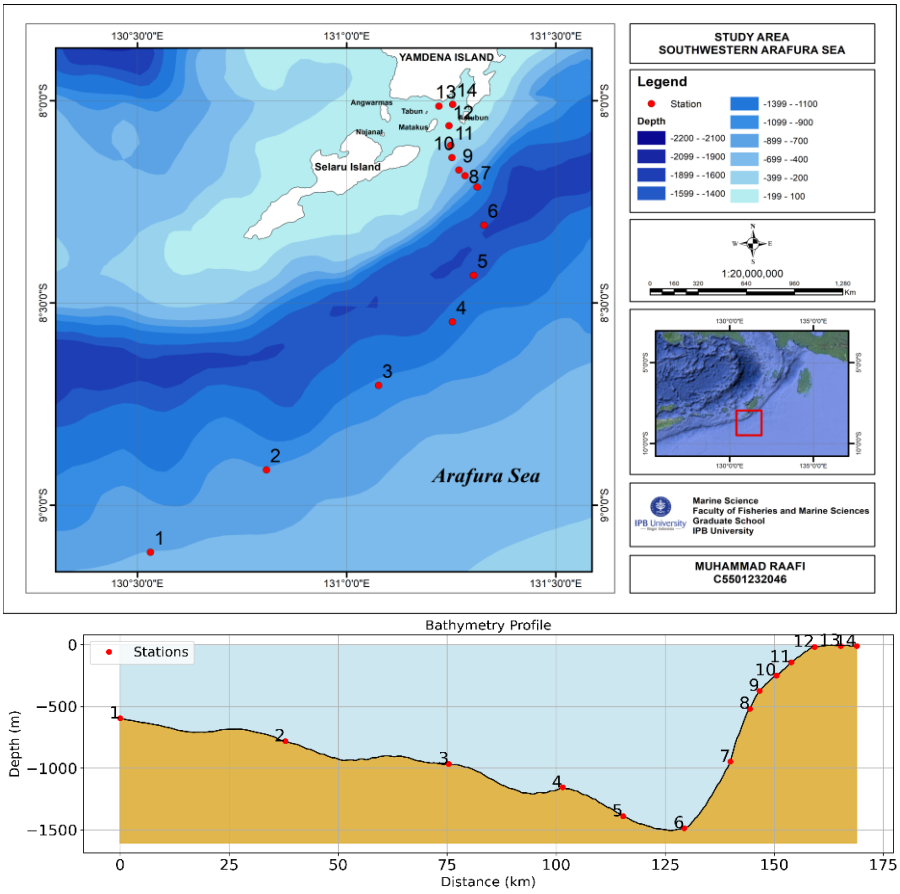

Figure 1. Study area (above) and cross-sectional bathymetric profile along the CTD stations (below) in the southwestern Arafura Sea.

Additional datasets were obtained from the Copernicus Marine Environment Monitoring Service (CMEMS) were used to complement the CTD observation data in the study area. One of the parameters analyzed was ocean current velocity (UV), which includes the northward (V) and eastward (U) current components, as well as temperature and salinity. These data were taken from the GLORYS12V1 product, a global reanalysis with a horizontal resolution of 1/12° and 50 vertical layers. The current data were downloaded in NetCDF format through CMEMS under DOI: https://doi.org/10.48670/moi-00021. The primary variables used in this study were the eastward and northward velocity components, and temperature for validation.

2.2. Methods

All data processing and analysis in this study were conducted using the Python programming language. The analysis was performed using several scientific computing libraries, including NumPy and Pandas for data processing, SciPy for signal processing, and Matplotlib for visualization. Seawater thermodynamic variables such as density, Brunt–Väisälä frequency (N^2), and Turner angle (Tu) were calculated using the Gibbs SeaWater (GSW) Oceanographic Toolbox for Python (IOC et al., 2010).

The indirect turbulence method used in this study was Thorpe analysis, a Python toolkit and the mixsea package. The toolkit was developed by Voet et al. (2015) to analyze turbulence parameters derived from the Thorpe-scale method, including Thorpe displacement, Thorpe scale (L_T), TKE dissipation rate (ε), and vertical eddy diffusivity ($K\rho$) and is available at https://mixsea.readthedocs.io/en/v0.2.0/. The input data consist of vertical density profiles obtained from CTD casts. The data underwent preprocessing to ensure quality and consistency before further analysis. The CTD profiles used in this study have a vertical resolution (dz) of 0.1 m.

Data validation was carried out to ensure that the identified overturns were physically reliable using the Galbraith–Kelley (GK) test, which evaluates temperature–salinity tightness. Overturns that did not meet seawater stability criteria were removed from further calculation to improve accuracy. In addition, two other tests proposed by (Gargett and Garner, 2008) were applied to distinguish real overturns from false overturns caused by noise or sensor spikes: the overturn ratio (Ro) and ΔN.

We applied the GK Test (Galbraith and Kelley, 1996) to detect and quantify overturning in CTD profiles. This test distinguishes true density inversions caused by turbulent mixing from instrumental noise by employing reordering analysis, run-length testing, and temperature–salinity (T–S) consistency checks. To further discriminate between real overturns and false overturns (e.g., due to sensor noise or salinity spikes), we adopted two additional tests, overturn ratio (Ro) and ΔN Test (Gargett and Garner, 2008). Ro is defined as the ratio of the vertical extent of positive and negative Thorpe displacements to the total patch thickness:

$$Ro = \left(\frac{L_+}{L}, \frac{L_-}{L}\right) \tag{1}$$

where $L+$ and $L-$ represent the vertical lengths of positive and negative displacements, and L is the overturn thickness. For an ideal overturn, $Ro \approx 0.5$ indicating symmetry. Smaller values suggest incomplete sampling or complex overturns, while $Ro < 0.2$ typically indicates false overturns caused by spurious spikes.

ΔN test evaluates T–S consistency within a patch using a double linear regression approach (Gargett and Garner, 2008; Ricker, 1973). The best-fit slope is determined as the geometric mean of regressions of T on S and S on T. After rotating the T–S coordinates, deviations perpendicular to the regression line (y-axis) are quantified:

$$\Delta N = y_M - y_m \tag{2}$$

where y_M and y_m are the largest positive and negative deviations, respectively. A small ΔN indicates that the overturn remains aligned with the local T–S relation, supporting its validity.

The analysis was then continued with the calculation of Thorpe displacement, Thorpe scale, Ozmidov scale, Brunt–Väisälä frequency, and estimation of TKE dissipation rate using mixsea. These steps were performed sequentially for each vertical profile at all sampling stations. The results produced vertical eddy diffusivity ($K\rho$), which form the basis for quantifying the magnitude of turbulent mixing at different depths.

Thorpe displacement is computed by sorting the measured density profile (ρ) obtained from CTD data to produce a stable density profile (ρs). Each water parcel undergoes a vertical displacement (d), defined as the distance between the parcel's original position (za) in the raw profile and its final position (zb) in the stable profile. This displacement represents the Thorpe displacement. After determining displacements (d) for all water parcels, the Thorpe scale is calculated as the root mean square of the vertical displacements ($d(z)$)(Thorpe, 1977):

$$L_T = \sqrt{\overline{d^2}} \tag{3}$$

The Brunt–Väisälä frequency (N^2) represents the natural oscillation of water parcels in a stably stratified water column and is calculated to evaluate water column stratification based on the vertical density gradient (Turner, 1973):

$$N^2 = \sqrt{-\frac{g}{\rho_0}\frac{\partial \rho}{\partial z}} \tag{4}$$

The estimation of TKE dissipation rate (ε) can be obtained by relating the Ozmidov scale (L_O) and the Thorpe scale (L_T). For simplicity, it is assumed that $L_O = cL_T$, where L_O represents the turbulent length scale determined by vertical displacements due to gravitational instability in the density profile. The TKE dissipation rate is then estimated as follows (Thorpe, 1977):

$$\varepsilon = cL_T^2 N^3 \tag{5}$$

where c is a freely adjustable parameter calibrated from microstructure-based ε measurements; in this study, a value of 0.8 was used (Dillon, 1982). With ε and N, the vertical eddy diffusivity is calculated using the following formulation (Osborn, 1980):

$$K\rho = \Gamma \frac{\varepsilon}{N^2} \tag{6}$$

Here, $K\rho$ is a parameter describing the efficiency of turbulent mixing in redistributing water mass properties such as temperature and salinity vertically. Γ represents the mixing efficiency, which is generally taken as 0.2 (Osborn, 1980), who suggested that the average mixing efficiency in the ocean is approximately 0.2.

Tidal signal analysis, including power spectral density (PSD) estimation, band-pass filtering around the semidiurnal M_2 frequency, and envelope extraction using the Hilbert transform, was performed using functions from the SciPy signal processing module. All figures and diagnostic plots were generated using Matplotlib in Python programming language. Sea-level tidal data were obtained from tidal predictions provided by the Indonesian Geospatial Information Agency (Badan Informasi Geospasial, BIG). The dominant tidal frequency was identified using power spectral density (PSD) analysis based on Welch's method, which estimates spectral energy by averaging modified periodograms to reduce variance and spectral leakage (Trauth, 2022). The PSD reveals a pronounced peak in the semidiurnal band, confirming the dominance of the M_2 tidal constituent. To examine temporal variability in tidal forcing, the M_2 component was isolated using a band-pass filter and its instantaneous amplitude was estimated using the Hilbert transform. Following standard discrete-time signal processing theory, the analytic signal is defined as

$$z(t) = x(t) + iH\{x(t)\} \tag{7}$$

where $x(t)$ is the band-limited M_2 signal and H denotes the Hilbert transform (Oppenheim et al., 1999). The M_2 envelope was obtained as the modulus of the analytic signal,

$A(t)=|z(t)|$, representing the time-varying amplitude of the semidiurnal tide. Envelope values were interpolated to the CTD sampling times and used as a proxy for relative tidal energy conditions during observations.

Linear theory of internal tide generation shows that internal tides are formed when the slope of the seafloor matches the slope of the internal tide ray path, and the internal tide forms a beam near its generation site through the superposition of many vertical modes (Lien and Gregg, 2001). The slope of the M_2 internal tide ray is:

$$c = \frac{dz}{dx} = \frac{\omega^2 - f^2}{N^2 - \omega^2} \quad (8)$$

With ω = tidal frequency (ω = 1.4×10−4 s−1 or M_2 tide), f = inertial frequency ($f = 2\Omega\sin\varphi$, with Ω = Earth's rotation rate and ϕ = latitude), N = local buoyancy frequency. Here, z is ocean depth and dz/dx is the bathymetric gradient. At locations where $|c - dz/dx|$ is minimal, tidal energy tends to be converted into internal wave energy, generating strong shear and enhancing TKE dissipation rate. Locations where the ray slope c closely matches the bottom slope are considered for internal tide generation and reflection, particularly under near-critical slope conditions. Using the vertical profile of N^2, ray path propagation was computed through stepwise integration along the horizontal and vertical directions, allowing the identification of potential reflection zones and regions of enhanced shear associated with internal tide–topography interactions (Naulita and Kitade, 2011).

3. Results and Discussion

3.1. Results

3.1.1. Temperature–Salinity Characteristics and Water Mass Identification

The Temperature–Salinity (T–S) diagram of the southwestern Arafura Sea, one of the main exit pathways of the Indonesian Throughflow (ITF), is shown in **Figure 2** and is overlaid with reference T–S data from the Banda Sea adapted from (Purwandana et al., 2020a). The diagram indicates that the water column is dominantly composed of Banda Sea Water (BSW) in the upper to intermediate layers and upper Indian Deep Water (upper IDW) in the deep layer.

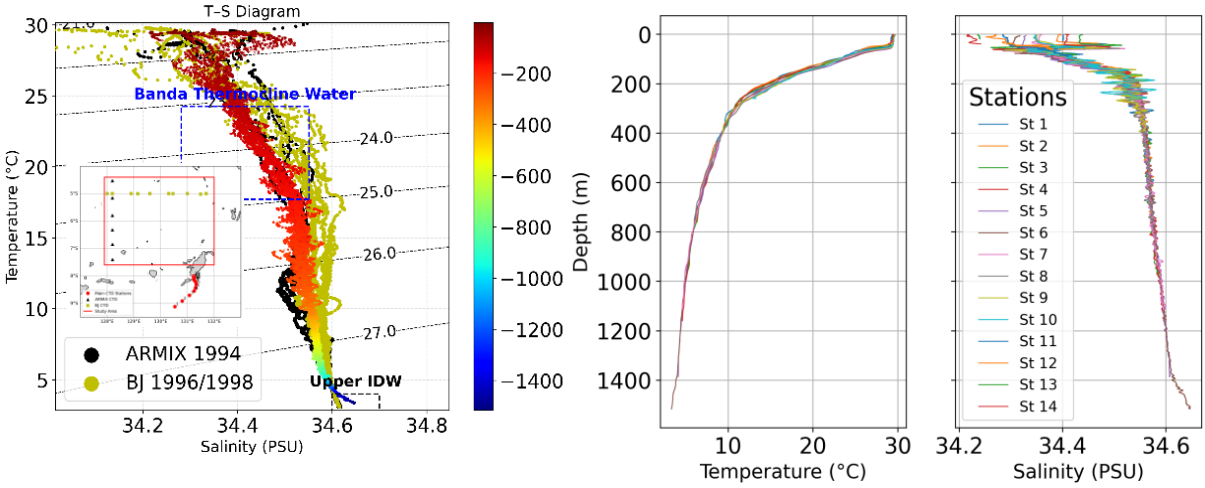

Figure 2. T-S diagram and vertical profiles of temperature and salinity in the southwestern Arafura Sea. The red box in the map indicates the Banda Sea region (from ARMIX and BJ expedition (Purwandana et al., 2020a)) used for comparison in the T–S diagram with yellow and black dots, while the red dots mark the CTD stations in the southwestern Arafura Sea.

Within the thermocline layer (approximately 200-300 m), salinity increases to around 34.6 psu, while temperature decreases rapidly, producing a marked density gradient. Distinct salinity extrema associated with North Pacific Intermediate Water (NPIW) are not observed.

Instead, this layer exhibits relatively homogeneous salinity across a density range of 23.5-26.5 σθ, characteristic of Banda Thermocline Water, which represents intermediate ITF waters that have undergone significant modification prior to reaching the southwestern Arafura Sea (Atmadipoera et al., 2022).

In the deep layer (>1,000 m), the water mass exhibits low temperatures (2-4 °C), relatively high salinity (34.6-34.7 psu), and high potential density (σθ ≈ 27.6), consistent with the characteristics of upper Indian Deep Water flowing northward from the Timor Trough (You, 2002; Atmadipoera et al., 2009). Below σθ >27.6 (approximately >1,400 m), the T–S characteristics are relatively uniform across stations, indicating a well-mixed deep layer that is consistent along both eastern and western ITF deep outflow pathways (Sprintall and Révelard, 2014).

Vertical temperature–salinity profiles also reveal salinity anomalies in the upper layer and near 200 m depth, where relatively saltier water overlies fresher water. These features are objectively observed in the profiles and indicate deviations from monotonic stratification within the upper thermocline.

3.1.2. Overturn Patch Validation

Even after applying optimal corrections, the density data from the CTD sensors still exhibited random noise and residual effects from salinity spiking. These disturbances can make perfectly mixed layers appear as if vertical rearrangement of water masses occurred. To avoid detecting false overturns, a filtering process was applied using the diagnostic parameters overturn ratio (*Ro*) and *ΔN*. Validation criteria followed thresholds of *ΔN* <0.003 and Ro >0.2 (Gargett and Garner, 2008), so only overturn patches meeting these conditions were recognized as real overturns.

As an example, Station 8, representing the slope region, demonstrates the validation process (**Figure 3**). From 340 initially detected patches, 310 passed the GK Test and vertical resolution criteria, while 30 were rejected. After applying the additional *ΔN* and *Ro* criteria, 259 patches were validated, and 81 were rejected.

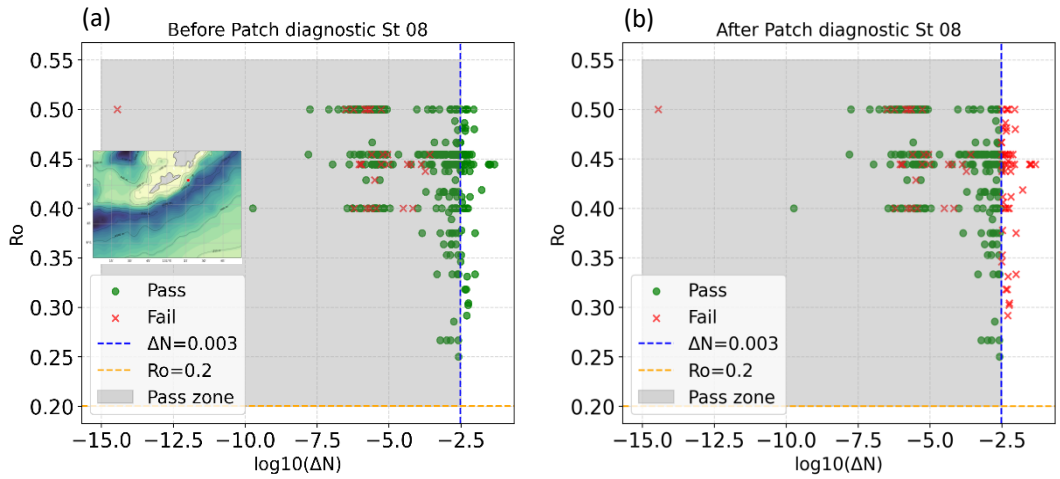

Figure 3. Comparison of diagnostic parameters (*Ro* and *ΔN*) at Station 8. The left panel represents the profiles after conventional quality control procedures (including GK Test and vertical resolution), while the right panel illustrates the refined profiles after applying Ro and *ΔN* based validation.

This comparison demonstrates that the validation process effectively filters out patches caused by noise, ensuring that only real overturns are used in calculating turbulence parameters. Consequently, the final results from Station 8 serve as the basis for confirming the reliability of the overturn identification method and the consistency of estimated turbulence parameters, such as the TKE dissipation rate (*ε*) and vertical eddy diffusivity (*Kρ*).

3.1.3. Thorpe Scale

The results of the Thorpe-scale analysis are shown in **Figure 4**. Overall, large overturning activity is primarily observed in the surface layer and near the seabed, which is consistent with the previously described stratification structure. In both layers, relatively weak stratification favors the development of gravitational instability and overturning. In the surface layer, enhanced overturning is associated with an actively mixed layer, where turbulent motions can develop over relatively large vertical scales. (Cisewski et al., 2005) showed that active mixed layers can generate substantial overturns before reaching the base of the mixed layer, reflecting elevated turbulent energy. In contrast, overturning activity generally decreases with depth as stratification strengthens.

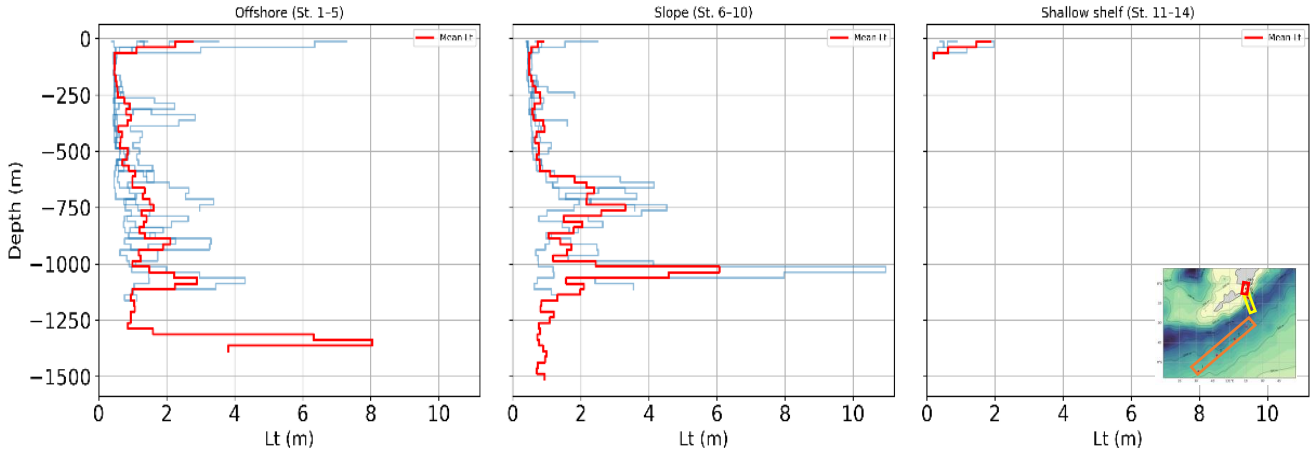

Figure 4. Thorpe scales (L_T) mean (red line) at representative stations in the southwestern Arafura Sea Station 1-5 (offshore; orange), Station 6-10 (slope; yellow), and Station 11-14 (shallow shelf; red). Blue lines show individual station profiles.

In the shallow shelf region (Stations 11-14), overturning activity is comparatively weak and sporadic. Thorpe scales are generally small and appear intermittently in the surface layer or at isolated depths, without a persistent vertical structure throughout the water column. This suggests that local turbulence in the shelf region is less effective at generating large overturns and is likely dominated by episodic processes, such as tidal intrusion, bottom-generated turbulence, or lateral mixing.

In the offshore region (Stations 1-5), overturning activity is relatively limited. Thorpe scales are generally small to moderate and are primarily concentrated near the surface (L_T 3 m) and close to the bottom (L_T 8 m). This pattern suggests that, despite the presence of instability, vertical mixing in the offshore region remains spatially constrained. In contrast, the slope region (Stations 6-10) exhibits markedly stronger overturning activity. Larger Thorpe scales (3-6 m) occur more frequently and extend from depths of approximately 600 m down to 1,000 m. This highlights the role of the continental slope as an efficient site of TKE dissipation rate, where interactions between tidal currents, internal waves, and steep topography promote the development of large-scale overturns. Similar enhancement of tidal-driven mixing over rough and sloping topography has been reported in previous studies (Nugroho et al., 2018; Robertson, 2023; van Haren et al., 2024).

3.1.4. Richardson Number

Richardson number (*Ri#*) calculations at Stations 1, 7, and 12 are shown in **Figure 5**, where patch-averaged buoyancy frequency (N^2) derived from CTD observations is plotted against shear (S^2) obtained from CMEMS reanalysis currents. This representation explicitly highlights the relative contribution of stratification and velocity shear in controlling flow stability.

Across all stations, most data points are distributed well above the critical *Ri#* thresholds (*Ri#* = 0.25 and *Ri#* = 0.5), indicating that water-column stability is primarily governed by

strong stratification rather than by shear intensity. In particular, the majority of patches cluster in regions of high N^2 and low S^2, implying that elevated *Ri#* values arise mainly from buoyancy effects.

At the offshore station (Station 1), several patches extend toward higher shear values and approach the critical Richardson number (*Ri#* ≈ 0.5). These patches are almost exclusively associated with the surface layer, where shear is enhanced by wind-driven circulation and surface currents. Below the surface mixed layer, however, Ri values remain high, indicating that stability (N^2) dominates over shear (S^2) throughout most of the water column, maintaining a generally stable stratification despite localized surface shear enhancement. The role of the gradient Richardson number as a proxy for turbulence suppression in stratified flows has been revisited in recent studies, showing that when $N^2 > S^2$ (*Ri#* >0.25), stratification effectively inhibits classical shear instabilities (Pelegrí et al., 2024)

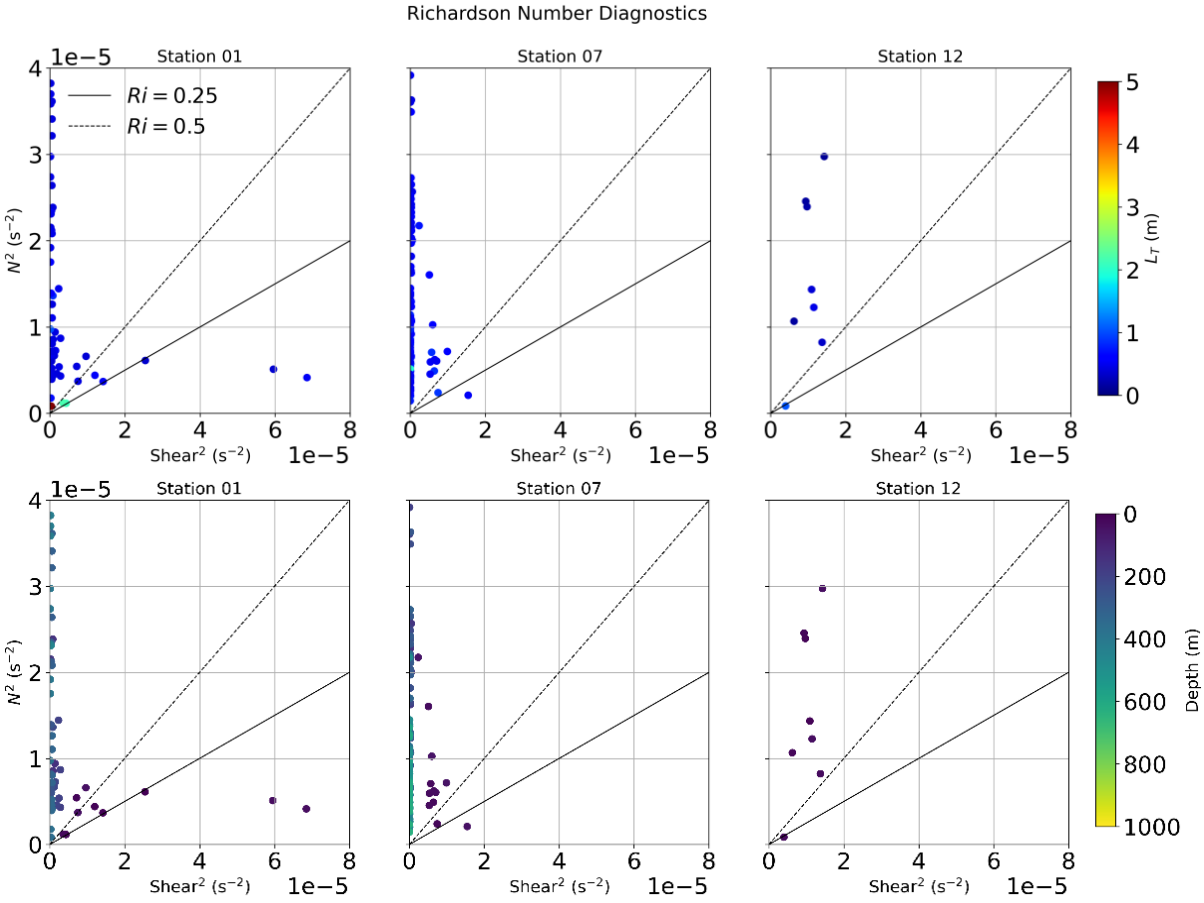

Figure 5. Richardson number diagnostics at Stations 1, 7, and 12 in the southwestern Arafura Sea. The upper panel shows scatter patches colored by the magnitude of the Thorpe scale (L_T), while the lower panel presents scatter patches colored by overturn depth.

At the slope station (Station 7), most patches show *Ri#* > 0.5, indicating a stratified water column. This stratification is primarily controlled by N^2 rather than shear. Although N^2 decreases substantially at depths of approximately 600-1,000 m, reflecting weaker stratification in the deeper layer, N^2 remains larger than shear² such that Ri values stay well above the critical threshold even at depth. Observational studies using in-situ shear and stratification data similarly show that stratification strongly influences local Ri and mixing regimes, with low *Ri#* (<0.25) occurring only where shear is unusually high relative to N^2 (Artana and Provost, 2023).

Despite the relatively small N^2 at these depths, large overturn scales are observed, suggesting that mixing at the slope station is not primarily shear-driven. Instead, it is likely associated with internal wave processes and internal tide interactions with steep topography, which can locally enhance turbulence without requiring strong background

shear. Such mechanisms have been documented in other oceanic contexts where shear instabilities extend below the thermocline under combined influences of internal waves and background currents (Magalhaes et al., 2025).

At the shallow shelf (Station 12), shear is smaller than N^2. Patches are dominated by high *Ri* values, far from the critical threshold, indicating a stable water column and minimal potential for shear-induced instability. This corresponds with the shallow and sheltered conditions around the Yamdena Islands, where available mixing energy is weaker.

Overall, the largest shear occurs in the surface layer. However, these calculations are based on CMEMS reanalysis data, which have coarser temporal and vertical resolution than required for turbulent-scale processes. Consequently, small-scale current variability is likely underrepresented, resulting in underestimated shear and *Ri#* values that appear more stable than the actual dynamic conditions, particularly in the physically active slope region.

3.1.5. Turner Angle

Based on the Richardson number analysis, the results indicate that overturn patches are primarily controlled by stratification rather than shear. Therefore, it is necessary to identify other factors that may trigger overturning within the water column. The Turner angle (*Tu*) is used to distinguish between stable and double-diffusive conditions (**Figure 6**).

Analysis of the Turner angle (*Tu*) reveals consistent signatures of double-diffusive processes across the three topographic regions (**Figure 6**). A prominent feature found at all stations is the presence of salt-fingering conditions in the upper thermocline (50-100 m), where *Tu* values exceed 45° or lie close to the threshold. This layer corresponds to the warm, high-salinity surface waters overlying cooler and fresher subsurface waters, which is also evident in the T–S diagrams (**Figure 2**). The vertical arrangement of saltier water above fresher water provides a density ratio conducive to salt fingering, suggesting that this process is widespread in the region.

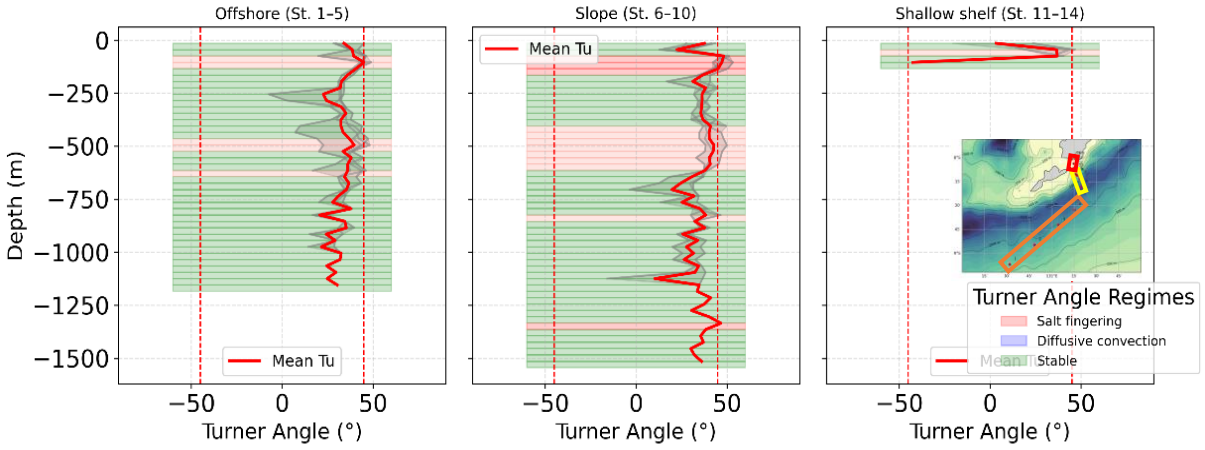

Figure 6. Turner angle (*Tu*) profiles for offshore (Stations 1-5; orange), slope (Stations 6-10; yellow), and shallow-shelf regions (Stations 11-14; red). Grey shade show min and max individual station profiles, the red line represents the mean *Tu*.

In the offshore region (Stations 1-5), *Tu* values mostly remain between 20° and 40°, indicating conditions approaching but not fully entering the salt-fingering regime. However, thin salt-fingering layers are detected near 500 m and 600 m, where the T–S diagram shows subtle intrusions of relatively saline intermediate water. These layers are weak and vertically limited, consistent with the generally stronger stratification and weaker water mass transformation offshore.

The slope region (Stations 6-10) exhibits the strongest and most vertically extensive salt-fingering signals. *Tu* values exceed 45° across a thick layer between 400-600 m, indicating vigorous double diffusion. Additional salt-fingering patches appear at ~1,300 m, coinciding with deep water masses (**Figure 2**). These features are consistent with water mass stacking

seen in the T–S diagrams, where high-salinity layers overlie lower-salinity intrusions. The enhanced occurrence of salt fingering along the slope suggests active vertical modification of water masses, potentially linked to internal tide–driven mixing pathways identified in the TKE dissipation rate analysis.

On the shallow continental shelf (Stations 11-14), *Tu* values remain mostly below 45°, reflecting a relatively stable water column shaped by limited water-mass diversity. Only the shallow 50 m layer exhibits salt-fingering signatures, consistent with the offshore and slope regions, but no deeper double-diffusive structures are present due to the limited depth and strong influence of surface-modified waters.

3.1.6. Internal Tide Ray Path

The tidal signal was analyzed to show the mechanisms of turbulent mixing. Tidal processes are known to generate internal waves through interactions between barotropic tidal motion and topographic features, which motivated the examination of tidal characteristics when assessing mixing conditions (Robertson and Ffield, 2008). Because internal waves occur at discrete tidal frequencies, the dominant barotropic constituent was identified to determine the frequency used in ray path modelling. **Figure 7** shows that the semidiurnal M_2 constituent (~12.42 h) is the most energetic component of the surface tidal signal, as indicated by a clear spectral peak in the PSD. After isolating the M_2 frequency using a narrow band-pass filter, we computed its instantaneous amplitude (the M_2 envelope), which represents the temporal variability of M_2 energy during the survey period. Several CTD casts in the slope region (Stations 6-10) coincided with elevated M_2-band amplitude, suggesting increased barotropic forcing at the time of sampling.

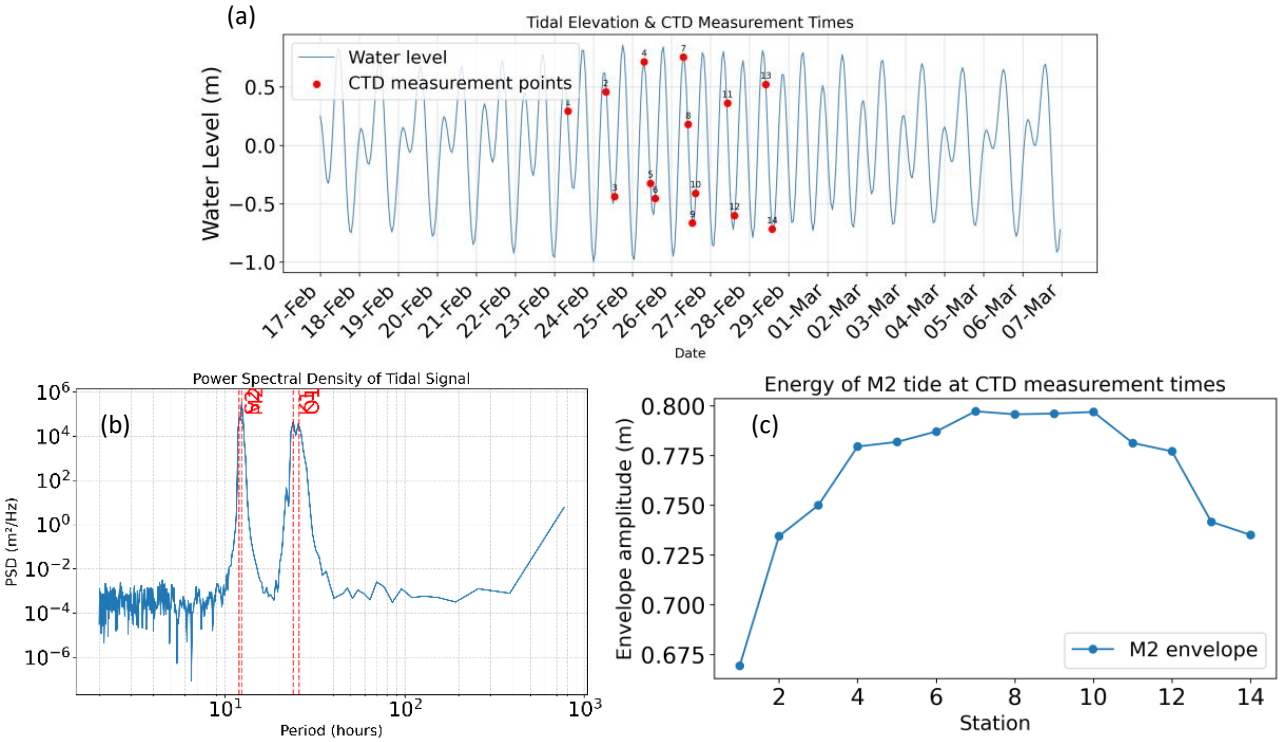

Figure 7. (a) Tidal Elevation, (b) Power spectral density of sea-level fluctuations and (c) semidiurnal M_2 band energy at CTD sampling times over the shelf region in the southwestern Arafura Sea.

Using this dominant frequency, together with the stratification (N^2), we constructed geometric ray paths to infer the likely propagation routes of M_2 internal tides. The resulting ray-tracing pattern indicates upslope and downslope propagation from regions of steep topography toward the interior basin—consistent with previous observations of internal tide generation and reflection along continental slopes (Nash et al., 2004). This supports the

interpretation that M_2 internal tides contribute to the distribution of TKE dissipation rate observed along the transect.

Elevated TKE dissipation rate ($\varepsilon \approx 10^{-7}$-$10^{-8}$ W kg^{-1}) aligns with the estimated M_2 internal tide ray paths near the slope and within the upper water column, indicating a strong coupling between internal tide propagation and turbulent mixing. As shown in **Figure 8**, deeper hotspots along the slope are more consistent with internal tide–driven mixing, whereas enhanced TKE dissipation rate near the surface is also modulated by wind and surface-wave processes. Similar turbulent features have been reported over continental shelves and slopes in other regions. Naulita (2014) identified several active turbulent layers over the shelf and slope, including mid-slope mixing layers ($\varepsilon > 10^{-6}$ W kg^{-1}) occurring at depths of ~255-440 m, well above the bottom and outside the characteristic ray paths of semidiurnal internal tides. These layers were therefore interpreted as being unrelated to bottom boundary layer friction or direct internal tide scattering, and instead associated with topographically induced turbulence. Such findings support the interpretation that elevated TKE dissipation rate observed away from the seabed and ray paths in the present study may arise from interactions between background stratification, complex topography, and internal wave energy.

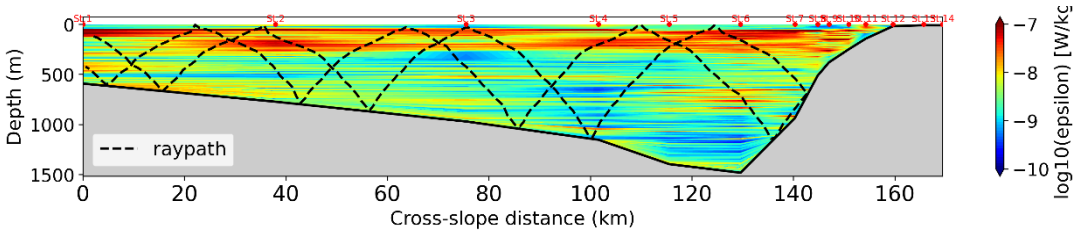

Figure 8. Cross-section of turbulent kinetic energy dissipation rate with M_2 ray path and seafloor topography in the southwestern Arafura Sea.

The vertical section of ε also shows localized intensification at mid–depths along steep topography. The internal tide ray paths derived from stratification (N^2) and the M_2 tidal frequency indicate multiple reflections along the slope, including downward turning at the lower flank, suggesting conditions approaching supercritical topography. Such reflection enhances shear and can promote overturning, which is consistent with the patches of elevated ε near 600-1,000 m. Although only CTD–based overturn estimates are available, the spatial coincidence between ray reflection zones and increased TKE dissipation rate suggests that part of the mixing is linked to tide–topography interaction. This mechanism is broadly consistent with previous studies showing that barotropic tides interacting with steep slopes can generate internal waves that transfer energy into the stratified interior and drive turbulent mixing (Daae et al., 2009; Naulita and Kitade, 2011; Klymak et al., 2012; MacKinnon et al., 2017).

A mechanism that can explain this pattern is the interaction of internal waves with a critical slope. When the seabed gradient approaches the characteristic slope of the incoming internal waves, the reflected wave energy becomes amplified, increasing shear and promoting turbulent overturns. Lien and Gregg (2001) demonstrated that under near-critical slope conditions, internal wave reflection intensifies the local energy flux, which enhances turbulent mixing within the pycnocline and along the slope boundary. This agrees with the observed band of elevated ε extending upward from the slope toward the surface, suggesting that a fraction of the TKE dissipation rate originates from slope-reflected internal waves rather than solely from breaking surface-generated waves.

Vertical eddy diffusivity ($K\rho$) varies strongly across the observation transect, with offshore values remaining very low ($<10^{-4}$ m^2 s^{-1}) due to pronounced stratification (**Figure 9**). In contrast, the slope region exhibits a sharp increase in $K\rho$, reaching ~10^{-3} m^2 s^{-1} at depths of 600-1,000 m, indicating more intense overturns and weakened stratification near the seabed, as shown in **Figure 8**.

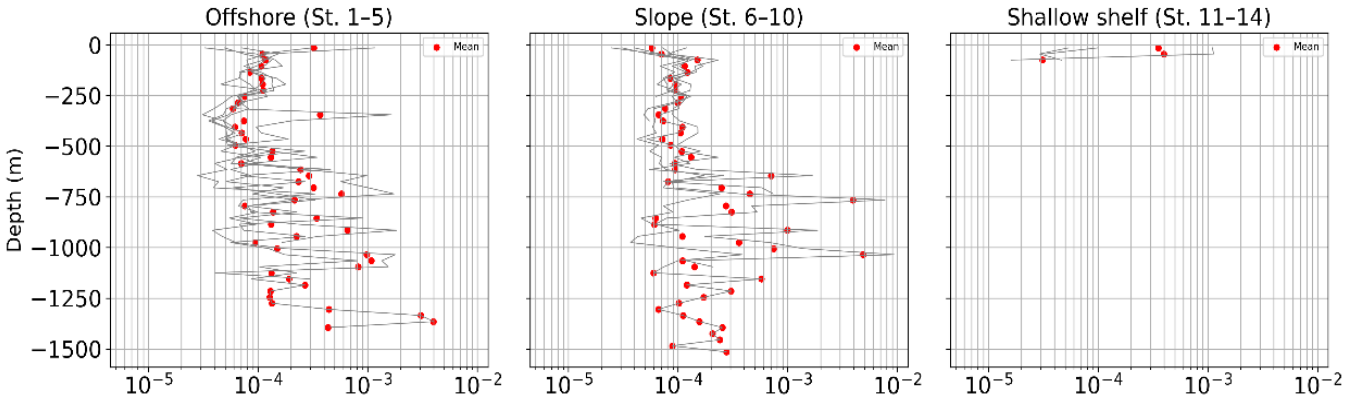

Figure 9. Cross-section of vertical eddy diffusivity ($K\rho$) across stations along the southwestern Arafura Sea.

Although the TKE dissipation rate analysis indicates energy supply in the surface layer, $K\rho$ remains low at the surface. This suggests that strong stratification in the upper layer limits mixing efficiency, even when energy is available from dynamic processes such as internal tides. These results are consistent with the ray path analysis, which shows that internal waves generated above steep topography are reflected and deformed before breaking at the slope. The trapped energy near the seabed is then converted into turbulence, producing a mixing hotspot along the slope.

3.2. Discussion

The results show that vertical mixing dynamics over the shelf region in the southwestern Arafura Sea are strongly influenced by a combination of stratification, double-diffusive instability, and the interaction of internal tides with bottom topography. Although turbulence appears in several layers, each mechanism operates differently in the offshore, slope, and shallow shelf regions.

3.2.1. Transformation of Southwestern Arafura Sea Water Masses

Previous studies have shown that the Banda Sea functions as a major transformation basin for the ITF, where incoming Pacific waters experience extensive modification of their temperature and salinity properties through prolonged residence time and interaction with complex basin geometry (Purwandana et al., 2020b; Atmadipoera et al., 2022). As a result, distinct thermohaline extrema associated with Pacific water masses are progressively eroded, producing relatively homogeneous Banda Sea Water that dominates the upper and thermocline layers downstream, as observed in this study.

The thermocline layer in the southwestern Arafura Sea is characterized by relatively uniform salinity within a broad density range (23.5-26.5 σθ) (**Figure 2**), consistent with the properties of Banda Thermocline Water reported in the Banda and Maluku Seas (Atmadipoera et al., 2022). The lack of identifiable NPIW features, such as a pronounced salinity minimum, indicates that intermediate Pacific waters have undergone significant transformation before reaching this region. Similar erosion of intermediate water mass signatures has been documented along other ITF pathways, highlighting the cumulative effect of water mass modification within the Indonesian Seas (Sprintall and Révelard, 2014; Purwandana et al., 2020b).

In the deep layer, the observed T–S properties are consistent with upper Indian Deep Water entering the region from the Indian Ocean via the Timor Trough. The relatively uniform deep-water characteristics across stations indicate that this water mass is well mixed horizontally and exhibits limited spatial variability within the southwestern Arafura Sea. This homogeneity is consistent with observations that deep ITF outflow waters maintain similar thermohaline properties along both eastern and western exit pathways toward the Indian Ocean (You, 2002; Atmadipoera et al., 2009).

The presence of salinity anomalies in the upper and thermocline layers, as revealed by the vertical T–S profiles, suggests localized deviations from idealized water mass structure. Such features have also been reported in previous studies of the Banda Sea and adjacent regions and are commonly interpreted as evidence of ongoing water mass transformation processes rather than the direct presence of distinct source waters. These anomalies further support the view that the southwestern Arafura Sea represents a downstream region where ITF waters have been substantially modified prior to their export into the Indian Ocean.

The buoyancy frequency (N^2) profile indicates that the thermocline layer at 50–200 m is the most strongly stratified zone along the transect. This stability makes the water column relatively resistant to mixing, particularly offshore and on the shallow shelf. low turbulent value ($K\rho < 10^{-6}$ m² s⁻¹) in these areas are consistent with this condition, showing that the available turbulent energy is not sufficient to overcome the restoring force of stratification. This means that although stratification is weaker than at the surface, there is still a significant vertical barrier to water-mass exchange. Intermediate N^2 values within this layer indicate a zone where internal turbulent energy may induce mixing. In other words, the thermocline acts as a barrier layer that slows the exchange of water masses between the surface and deeper layers. As described by (Saha et al., 2021), a barrier layer prevents mixing between the mixed layer and the thermocline, limiting the influence of freshwater, heat, and momentum fluxes from the surface, and trapping heat and salinity in the upper layer.

In contrast, very low N^2 in the lower slope indicates weakened stratification at 600–1,000 m depth. This condition supports the development of large overturning patches detected from Thorpe analysis and increases vertical eddy diffusivity up to 10^{-3} m² s⁻¹. Thus, the slope acts as a critical zone where tidal energy and momentum are transferred into effective turbulence.

3.2.2. Shear Instability and Role of Double Diffusion Across Regions

Most Richardson number values exceed the critical limit of *Ri#* = 0.25 (**Figure 5**), indicating that shear is not the primary trigger for instability. Although some surface patches approach the critical threshold, the shear was estimated using CMEMS data with coarse spatial and vertical resolution, which may not capture small-scale turbulence. This suggests that surface shear contributes, but is insufficient to explain the large overturns, particularly in deeper layers. Although the Richardson number computed from model-derived velocity suggests weak background shear, it does not fully explain the presence of strong overturns in the slope region. The lack of clear shear signatures implies that additional mechanisms must be contributing to the enhanced mixing. To address this gap, Turner angle analysis was used to diagnose double-diffusive processes across the water column.

The Turner angle results reveal that salt fingering is a prominent mechanism within the thermocline and mid-depth layers of the slope region, consistent with the T–S structure (**Figure 2**) showing warm, saline layers overlying cooler, fresher waters. These conditions promote double-diffusive instability, providing an alternative mixing pathway that does not rely on shear. Salt-fingering and other double-diffusive processes have been shown to contribute to vertical mixing, particularly where heat diffuses faster than salt and the stratification is conducive (Girishkumar et al., 2024; Li et al., 2025). However, the process exhibits strong spatial variability. In the offshore and shallow shelf regions, *Tu* values approach the salt-fingering threshold but rarely exceed 45°, indicating that double diffusion is present but weak and insufficient to generate substantial mixing. This is consistent with the relatively homogeneous water masses in shallow settings and the limited intrusion of high-salinity intermediate waters.

Incorporating stratification data from the buoyancy frequency (N^2) in *Ri#* plots (**Figure 5**) reveals that at approximately 50-200 m is the most strongly stratified zone along the stations. Strong stratification in this zone inhibits vertical exchange, resulting in comparatively low turbulent value ($K\rho < 10^{-6}$ m² s⁻¹) offshore and on the shallow shelf, consistent with weak turbulent energy available to overcome the restoring force of stratification (Shang et al., 2017). Although stratification above this layer is weaker than

near the surface, it still presents a significant vertical barrier to water-mass exchange. Intermediate N^2 values within the thermocline indicate a region where ambient turbulent energy may induce partial mixing, but only when supplementary mechanisms (e.g., internal waves or double diffusion) are present. In this regard, the thermocline acts as a barrier layer that limits the downward propagation of surface turbulence and traps heat and salinity in the upper layer (similar to barrier layers described in tropical ocean studies (Saha et al., 2021).

In contrast, very low N^2 values in the lower slope region, particularly at depths of about 600-1,000 m, indicate weakened stratification. Under these conditions, the water column becomes less resistant to vertical displacement, supporting the development of large overturning patches detected from Thorpe analysis. This reduced stratification in the deep slope region is associated with increased vertical eddy diffusivity, in some instances approaching values as high as ~10^{-3} m² s^{-1}, which aligns with observed enhanced mixing over rough bathymetry and near internal-wave generation sites in other ocean regions (Tweddle et al., 2013; Shang et al., 2017; Takahashi et al., 2024). Thus, the slope acts as a critical zone where tidal energy and momentum can be converted into effective turbulence when stratification is sufficiently relaxed.

3.2.3. Internal Tides as a Driver of Enhanced Slope Mixing

M_2 ray path analysis based on the observed stratification (N^2) and M_2 tidal frequency suggests that internal tides may act as a significant pathway for energy toward the slope region (**Figure 8**). When barotropic tidal currents interact with steep topography, internal waves can be partially reflected both upward and downward, depending on whether the seabed is subcritical or supercritical. In the present study, the continental slope is steep enough to be locally supercritical, which makes downward reflection plausible.

By sampling the M_2 envelope at the CTD cast times (and applying a plausible travel-time shift based on estimated group speeds), we found that casts with elevated TKE dissipation rate ($\varepsilon \approx 10^{-7}$-$10^{-8}$ W kg^{-1}) often coincide with peaks in the M_2 envelope shifted for travel time (**Figure 7**). This temporal alignment suggests that strong barotropic forcing at M_2 may lead to baroclinic internal wave arrival and subsequent mixing near the slope, even though the instantaneous surface elevation may be decreasing. This behavior echoes the mechanism described by (Nash et al., 2004; Marques et al., 2024), where semidiurnal internal tides interacting with super-critical slopes generate strong shear and TKE dissipation rate independent of immediate tidal height.

This interpretation is consistent with the ε distribution. The slope exhibits elevated TKE dissipation rate values of approximately 10^{-7}-10^{-8} W kg^{-1}, higher than the surrounding deep basin, indicating that part of the turbulent energy may originate from internal wave reflection or breaking rather than background mixing alone. Similar processes have been documented in narrow straits with steep sills, where tide–topography interactions produce strong turbulence. For example, (Nagai et al., 2021) reported that a supercritical sill in the Manipa Strait generated a downslope jet and large density overturns, accompanied by TKE dissipation rate exceeding 10^{-5} W kg^{-1}. While the present dataset does not directly observe currents or jets, the elevated ε values and overturn signals near the slope are qualitatively consistent with internal tide–induced mixing.

These findings align with theoretical and numerical studies showing that supercritical topography tends to reflect low-mode internal tides back into deeper water, concentrating energy along ray paths (MacKinnon et al., 2017). Such downward reflection enhances local shear and promotes mixing even without strong surface signatures, explaining why ε increases near the slope while the overlying water column remains strongly stratified.

Near the surface, ε also shows elevated values, but $K\rho$ remains low, indicating that turbulence does not effectively mix density surfaces (**Figure 9**). This pattern suggests stratification-limited mixing and partial reflection of internal wave energy. Overall, the combined evidence indicates that the slope area likely acts as a localized mixing hotspot where internal tide energy interacts with steep topography and stratification.

3.2.4. Integrated Mixing Mechanisms in the Southwestern Arafura Sea

The results indicate that turbulent mixing in the southwestern Arafura Sea arises from the combined influence of background stratification, double-diffusive instability, and internal tide-topography interaction. These processes operate at different depths and spatial locations, together shaping the vertical structure of mixing along the observational stations.

Table 1. Representative values of vertical eddy diffusivity ($K\rho$) for stratified, salt-fingering, and slope mixing layers.

Layer	Repesentative Stations	Depth	Mean $K\rho$ ($m^2\ s^{-1}$)	Median $K\rho$ ($m^2\ s^{-1}$)
Strongly Stratified	Station 11	50-100 m	1.60×10^{-5}	9.86×10^{-6}
Salt Fingering	Station 6	500-550 m	5.79×10^{-5}	5.71×10^{-5}
Slope Region	Station 7	1,000-1,050 m	7.55×10^{-3}	9.61×10^{-3}

Stratification provides the primary control on the vertical distribution of mixing. Weak vertical eddy diffusivity is observed in the shallow shelf waters near Station 11 (50-100 m), where the median $K\rho$ is on the order of 10^{-6} $m^2\ s^{-1}$ (**Table 1**). Despite the relatively shallow depth, the water column remains strongly stratified, and the vertical density gradient suppresses large vertical displacements and limits turbulent exchange. Such conditions indicate that stratification acts as an effective barrier layer that inhibits vertical mixing even in shallow shelf environments.

Within this stratified background, double-diffusive processes contribute to vertical property exchange. Turner angle diagnostics indicate salt-fingering conditions in intermediate layers between 500-550 m depth. Representative values from Station 6 show median $K\rho$ on the order of 10^{-5} $m^2\ s^{-1}$ (**Table 1**), suggesting relatively weak but persistent vertical exchange associated with double diffusion. The similarity of $K\rho$ values between the salt-fingering layer and the upper stratified layer indicates that double diffusion contributes only modestly to the overall mixing budget compared with more energetic turbulence mechanisms.

In contrast, the strongest mixing occurs along the continental slope. Station 7 is located adjacent to the slope region and weak stratification provides suitable observations for examining slope-related mixing processes. At the stations, vertical eddy diffusivity increases at depths of 1,000-1,050 m. In these layers, the median $K\rho$ reaches values on the order of 10^{-3} $m^2\ s^{-1}$ (**Table 1**), which is roughly two to three orders of magnitude larger than those observed in the upper stratified and salt-fingering layers. Such elevated vertical eddy diffusivity coincides with large Thorpe overturns and enhanced TKE dissipation rate ($\varepsilon \approx 10^{-7}$-$10^{-8}$ W kg^{-1}), indicating intense turbulent mixing.

The primary energy source driving this enhanced mixing is likely associated with internal tide-topography interaction. Ray path analysis based on the dominant M_2 tidal frequency suggests that internal tides generated over steep bathymetry propagate and reflect along the continental slope, concentrating internal wave energy within the mid-depth water column. The spatial correspondence between internal tide ray paths, elevated TKE dissipation rate, and large overturning scales supports the interpretation that internal wave reflection and breaking play a major role in generating turbulence in this region.

Taken together, these results suggest a hierarchical mixing framework in which internal tides supply the dominant turbulent energy, stratification regulates where this energy can effectively generate mixing, and double diffusion contributes locally to vertical property exchange. The continental slope therefore acts as a mixing hotspot where these mechanisms interact, resulting in substantially enhanced turbulent mixing compared with the surrounding offshore and shelf waters.

3.2.5. Implications, Uncertainties, and Future Work

Nevertheless, several caveats remain. The M_2 ray path calculation uses a simplified geometric approximation and does not explicitly model modal energy partitioning, rotation, or amplitude attenuation. The envelope at the surface serves only as a proxy for internal tide energy. Direct measurements of baroclinic velocity fields would be required for definitive attribution. Future work should employ moored ADCPs or microstructure profilers to validate the timing and spatial distribution of internal-tide energy flux and TKE dissipation rate. Because only hydrographic (CTD) observations are available, the proposed mechanism cannot be confirmed directly. However, the turbulence and stratification patterns are consistent with the internal tide–topography interaction documented in previous studies, including those in steep-slope and sill environments.

4. Conclusions

This study shows that vertical mixing in the southwestern Arafura Sea is strongly controlled by the combined effects of stratification and topographic forcing. Offshore and shallow shelf waters remain strongly stratified, resulting in weak vertical mixing with vertical eddy diffusivity on the order of 10^{-6} m^2 s^{-1}. In contrast, weakened stratification near the continental slope allows large overturning events and intense turbulence, producing vertical eddy diffusivity reaching 10^{-3} m^2 s^{-1}. Salt-fingering conditions are present in intermediate layers and contribute modestly to vertical exchange, although their associated vertical eddy diffusivity remains relatively weak compared with turbulence generated in the slope region.

The results suggest that internal tide–topography interaction is the dominant mechanism driving enhanced mixing along the slope. Internal tide ray path analysis indicates that energy generated over steep bathymetry can propagate and reflect within the water column, concentrating turbulence in mid-depth layers. Consequently, the continental slope acts as a mixing hotspot that significantly enhances vertical exchange compared with the surrounding offshore and shelf waters.

This study also provides new insight into the mixing dynamics of the southwestern Arafura Sea, a region that has received limited attention in previous turbulence studies. By combining Thorpe-scale turbulence analysis with Richardson number diagnostics, Turner angle evaluation, and internal-tide ray path modeling, this study provides an integrated framework for interpreting the interaction between stratification, double diffusion, and internal tide processes in controlling vertical mixing.

However, several limitations should be acknowledged. The analysis relies primarily on hydrographic (CTD) observations and therefore cannot directly resolve velocity fields or internal-wave energy flux. In addition, the internal-tide ray path analysis represents a simplified geometric approximation and does not explicitly account for modal energy partitioning or rotational effects. Future studies employing moored ADCP observations or microstructure turbulence measurements would be necessary to directly quantify internal-tide energy flux and TKE dissipation rate in this region

Conflicts of Interest

There are no conflicts to declare.

Acknowledgements

The authors would like to express their sincere gratitude to INPEX Masela Ltd. for providing access to the CTD dataset used in this study. The CTD measurements were part of the metocean survey conducted to support the Front End Engineering Design (FEED) for the development of the Abadi Field.

AI Writing Statement

During the preparation of this work, the author(s) used chatGPT tools for language refinement during the preparation of this manuscript. After using this tool/service, the author(s) reviewed and edited the content as needed and take(s) full responsibility for the content of the publication.

References

Acabado, C.S., Cheng, Y.H., Chang, M.H., & Chen, C.C. (2021). Vertical Nitrate Flux Induced by Kelvin–Helmholtz Billows Over a Seamount in the Kuroshio. *Frontiers in Marine Science*, *8*(680729(, 1-14. https://doi.org/10.3389/fmars.2021.680729

Artana, C., & Provost, C. (2023). Intense anticyclones at the global Argentine Basin array of the Ocean Observatory Initiative. *Ocean Science, 19*(3), 953-971. https://doi.org/10.5194/os-19-953-2023

Atmadipoera, A.S., Koch-Larrouy, A., Madec, G., Grelet, J., Baurand, F., Jaya, I., & Dadou, I. (2022). Part I: Hydrological properties within the eastern Indonesian throughflow region during the INDOMIX experiment. *Deep-Sea Research Part I: Oceanographic Research Papers*, *182*. https://doi.org/10.1016/j.dsr.2022.103735

Atmadipoera, A.S., Molcard, R., Madec, G., Wijffels, S., Sprintall, J., Koch-Larrouy, A., Jaya, I., & Supangat, A. (2009). Characteristics and variability of the Indonesian throughflow water at the outflow straits. *Deep-Sea Research Part I: Oceanographic Research Papers*, *56*(11), 1942-1954. https://doi.org/10.1016/j.dsr.2009.06.004

Capuano, T.A., Nugroho, D., Koch-larrouy, A., Dadou, I., Zaron, E., Vantrepotte, V., Allain, D., & Kien, T. (2022). Impact of internal tides on distributions and variability of Chlorophyll-a and Nutrients in the Indonesian Seas. *Journal of Geophysical Research*. https://doi.org/10.1002/essoar.10512046.1

Cisewski, B., Strass, V.H., & Prandke, H. (2005). Upper-ocean vertical mixing in the Antarctic Polar Front Zone. *Deep-Sea Research Part II: Topical Studies in Oceanography*, *52*(9-10 SPEC. ISS.), 1087-1108. https://doi.org/10.1016/j.dsr2.2005.01.010

Daae, K.L., Fer, I., & Povl Abrahamsen, E. (2009). Mixing on the continental slope of the southern Weddell Sea. *Journal of Geophysical Research: Oceans*, *114*(9), 1-13. https://doi.org/10.1029/2008JC005259

Dillon, T.M. (1982). Vertical overturns: A comparison of Thorpe and Ozmidov length scales. *Journal of Geophysical Research: Oceans*, *87*(C12), 9601-9613. https://doi.org/10.1029/jc087ic12p09601

Estrada-Allis, S.N., Rodríguez-Santana, Á., Naveira-Garabato, A.C., García-Weil, L., Arcos-Pulido, M., & Emelianov, M. (2023). Enhancement of turbulence and nutrient fluxes within an Eastern Boundary Upwelling Filament: a diapycnal entrainment approach. *Frontiers in Marine Science*, *10*, 1-20. https://doi.org/10.3389/fmars.2023.1113879

Galbraith, P.S., & Kelley, D.E. (1996). Identifying overturns in CTD profiles. *Journal of Atmospheric and Oceanic Technology*, *13*(3), 688-702. https://doi.org/10.1175/1520-0426(1996)013<0688:IOICP>2.0.CO;2

Gargett, A., & Garner, T. (2008). Determining Thorpe scales from ship-lowered CTD density profiles. *Journal of Atmospheric and Oceanic Technology*, *25*(9), 1657-1670. https://doi.org/10.1175/2008JTECHO541.1

Girishkumar, M.S., Ashin, K., & Rama Rao, E.P. (2024). Diapycnal mixing induced by salt finger and internal tides on the northwest coast of India. *Continental Shelf Research*, *273*, 105172. https://doi.org/https://doi.org/10.1016/j.csr.2024.105172

IOC, SCOR, & IAPSO. (2010). The international thermodynamic equation of seawater – 2010: Calculation and use of thermodynamic properties. *Intergovernmental Oceanographic Commission, Manuals and Guides No. 56*, *June*, 196.

Kämpf, J. (2015). Undercurrent-driven upwelling in the northwestern Arafura Sea. *Geophysical Research Letters*, *42*(21), 9362-9368. https://doi.org/10.1002/2015GL066163

Klymak, J.M., Legg, S., Alford, M.H., Buijsman, M., Pinkel, R., & Nash, J.D. (2012). The direct

breaking of internal waves at steep topography. *Oceanography*, *25*(2), 153-159. https://doi.org/10.5670/oceanog.2012.50

Kobari, T., Honma, T., Hasegawa, D., Yoshie, N., Tsutsumi, E., Matsuno, T., Nagai, T., Kanayama, T., Karu, F., Suzuki, K., Tanaka, T., Guo, X., Kume, G., Nishina, A., & Nakamura, H. (2020). Phytoplankton growth and consumption by microzooplankton stimulated by turbulent nitrate flux suggest rapid trophic transfer in the oligotrophic Kuroshio. *Biogeosciences*, *17*(9), 2441-2452. https://doi.org/10.5194/bg-17-2441-2020

Li, J., Yang, Q., & Sun, H. (2025). Dissipation ratio and eddy diffusivity of turbulent and salt finger mixing derived from microstructure measurements. *Oceanic Science, 21*(22), 829-849. https://doi.org/10.5194/os-21-829-2025

Lien, R.C., & Gregg, M.C. (2001). Observations of turbulence in a tidal beam and across a coastal ridge. *Journal of Geophysical Research: Oceans*, *106*(C3), 4575-4591. https://doi.org/10.1029/2000JC000351

Mackinnon, J.A., Alford, M.H., Sun, O., Pinkel, R., Zhao, Z., & Klymak, J. (2013). Parametric subharmonic instability of the internal tide at 29°N. *Journal of Physical Oceanography*, *43*(1), 17-28. https://doi.org/10.1175/JPO-D-11-0108.1

MacKinnon, J.A., Zhao, Z., Whalen, C.B., Waterhouse, A.F., Trossman, D.S., Sun, O.M., St Laurent, L.C., Simmons, H.L., Polzin, K., Pinkel, R., Pickering, A., Norton, N. J., Nash, J.D., Musgrave, R., Merchant, L.M., Melet, A.V., Mater, B., Legg, S., Large, W.G., … Alford, M.H. (2017). Climate process team on internal wave-driven ocean mixing. *Bulletin of the American Meteorological Society*, *98*(11), 2429-2454. https://doi.org/10.1175/BAMS-D-16-0030.1

Magalhaes, J.M., Coubard, M.J., B, C., da Silva, J.C.B, Buijsman, M.C., Santos, A.I., Amorim, A., & Oliveira, P.B. (2025). Shear instabilities in Internal Solitary Waves under high and low-wind regimes. *Continental Shelf Research, 295*(January). https://doi.org/10.1016/j.csr.2025.105561

Marques, O.B., Alford, M.H., Pinkel, R., Mackinnon, J.A., Voet, G., Klymak, J.M., & Nash, J.D. (2024). Observations of Tidally Driven Turbulence Over Steep, Small-Scale Topography Embedded in the Tasman Slope. *Journal of Physical Oceanography*, *54*(2), 601–615. https://doi.org/10.1175/JPO-D-23-0038.1

Nagai, T., Hibiya, T., & Syamsudin, F. (2021). Direct Estimates of Turbulent Mixing in the Indonesian Archipelago and Its Role in the Transformation of the Indonesian Throughflow Waters. *Geophysical Research Letters*, *48*(6), 1-9. https://doi.org/10.1029/2020GL091731

Nash, J.D., Kunze, E., Toole, J.M., & Schmitt, R.W. (2004). Internal Tide Reflection and Turbulent Mixing on the Continental Slope. *Journal of Physical Oceanography, 34*(5), 1117-1134. https://doi.org/10.1175/1520-0485(2004)034%3C1117:ITRATM%3E2.0.CO;2

Naulita, Y. (2014). Percampuran Turbulen yang dipicu Topografi di Perairan Paparan Kontinen Jogashima, Teluk Sagami, Jepang. *Jurnal Ilmu Dan Teknologi Kelautan Tropis*, *6*(2), 479-490. https://doi.org/https://doi.org/10.29244/jitkt.v6i2.9023

Naulita, Y., & Kitade, Y. (2011). Observed Turbulence Properties Over the Continental Shelf and Slope Off. *La Mer*, *49*, 1-15. https://www.researchgate.net/publication/281255387

Nugroho, D., Koch-Larrouy, A., Gaspar, P., Lyard, F., Reffray, G., & Tranchant, B. (2018). Modelling explicit tides in the Indonesian seas: An important process for surface sea water properties. *Marine Pollution Bulletin*, *131*, 7-18. https://doi.org/10.1016/j.marpolbul.2017.06.033

Oppenheim, A.V, Schafer, R.W., & Buck, J.R. (1999). *Discrete-Time Signal Processing* (Second Edi). Upper Saddle River, New Jersey: Prentice-Hal, Inc.

Osborn, T.R. (1980). Estimates of the Local Rate of Vertical Diffusion from Dissipation Measurements. *Journal of Physical Oceanography*, *10*(1), 83-89. https://doi.org/10.1175/1520-0485(1980)010%3C0083:EOTLRO%3E2.0.CO;2

Pelegrí, J.L., Claret, M., & Sangrà, P. (2024). Vertical Shear, Diapycnal Shear and the Gradient Richardson Number. *Oceans*, *5*(4), 785-804. https://doi.org/10.3390/oceans5040045

Purwandana, A., Cuypers, Y., Bouruet-Aubertot, P., Nagai, T., Hibiya, T., & Atmadipoera, A.S. (2020a). Historical CTD dataset and associated processed dissipation rate using an improved Thorpe method in the Indonesian seas. *Data in Brief*, *30*. https://doi.org/10.1016/j.dib.2020.105519

Purwandana, A., Cuypers, Y., Bouruet-Aubertot, P., Nagai, T., Hibiya, T., & Atmadipoera, A.S. (2020b). Spatial structure of turbulent mixing inferred from historical CTD datasets in the Indonesian seas. *Progress in Oceanography*, *184*. https://doi.org/10.1016/j.pocean.2020.102312

Ricker, W.E. (1973). Linear regressions in flshery research. *Journal Fisheries Research Board of Canada*, *30*(3), 409-434. https://doi.org/10.1139/f73-072

Robertson, R. (2023). Tidal and internal tidal impacts in the Tasman Sea. *Geoscience Letters*, *10*(8), 1-19. https://doi.org/10.1186/s40562-023-00262-1

Robertson, R., & Ffield, A. (2008). Baroclinic tides in the Indonesian seas: Tidal fields and comparisons to observations. *Journal of Geophysical Research: Oceans*, *113*(7). https://doi.org/10.1029/2007JC004677

Saha, A., Serra, N., & Stammer, D. (2021). Growth and Decay of Northwestern Tropical Atlantic Barrier Layers. *Journal of Geophysical Research: Oceans*, *126*(5). https://doi.org/10.1029/2020JC016956

Shang, X.D., Liang, C.R., & Chen, G.Y. (2017). Spatial distribution of turbulent mixing in the upper ocean of the South China Sea. *Ocean Science*, *13*(3), 503-519. https://doi.org/10.5194/os-13-503-2017

Sprintall, J., & Révelard, A. (2014). The Indonesian Throughflow response to Indo-Pacific climate variability. *Journal of Geophysical Research: Oceans*, *119*(2), 1161-1175. https://doi.org/10.1002/2013JC009533

Takahashi, A., Lien, R.C., Kunze, E., Ma, B., Nakamura, H., Nishina, A., Tsutsumi, E., Inoue, R., Nagai, T., & Endoh, T. (2024). Energetic Stratified Turbulence Generated by Kuroshio–Seamount Interactions in Tokara Strait. *Journal of Physical Oceanography*, *54*(2), 461-484. https://doi.org/10.1175/JPO-D-22-0242.1

Thorpe, S.A. (1977). Turbulence and mixing in a Scottish Loch. *Philosophical Transactions of the Royal Society of London. Series A, Mathematical and Physical Sciences*, *286*(1334), 125-181. https://doi.org/10.1098/rsta.1977.0112

Trauth, M.H. (2022). *Python Recipes for Earth Sciences*. Springer Textbooks in Earth Sciences, Geography and Environment. Cham, Switzerland: Springer Cham.

Tsutsumi, E., Matsuno, T., Itoh, S., Zhang, J., Senjyu, T., Sakai, A., Lee, K., Yanagimoto, D., Yasuda, I., Ogawa, H., & Villanoy, C. (2020). Vertical fluxes of nutrients enhanced by strong turbulence and phytoplankton bloom around the ocean ridge in the Luzon Strait. *Scientific Reports*, *10*(1). https://doi.org/10.1038/s41598-020-74938-5

Turner, J.S. (1973). *Bouyancy Effects in Fluids*. Cambridge, United Kingdom: Cambridge University Press.

Tweddle, J.F., Sharples, J., Palmer, M.R., Davidson, K., & McNeill, S. (2013). Enhanced nutrient fluxes at the shelf sea seasonal thermocline caused by stratified flow over a bank. *Progress in Oceanography*, *117*, 37-47. https://doi.org/10.1016/j.pocean.2013.06.018

van Haren, H., Voet, G., Alford, M.H., Fernández-Castro, B., Naveira Garabato, A.C., Wynne-Cattanach, B.L., Mercier, H., & Messias, M.J. (2024). Near-slope turbulence in a Rockall canyon. *Deep-Sea Research Part I: Oceanographic Research Papers*, *206*, 1-14. https://doi.org/10.1016/j.dsr.2024.104277

Voet, G., Girton, J.B., Alford, M.H., Carter, G.S., Klymak, J.M., & Mickett, J.B. (2015). Pathways, volume transport, and mixing of abyssal water in the Samoan Passage. *Journal of Physical Oceanography*, *45*(2), 562-588. https://doi.org/10.1175/JPO-D-14-0096.1

Yang, W., Wei, H., Zhao, L., & Zhang, J. (2020). Turbulence and vertical nitrate flux adjacent to the Changjiang Estuary during fall. *Journal of Marine Systems*, *212*. https://doi.org/10.1016/j.jmarsys.2020.103427

You, Y. (2002). A global ocean climatological atlas of the Turner angle: Implications for double-diffusion and water-mass structure. *Deep-Sea Research Part I: Oceanographic Research Papers*, *49*(11), 2075-2093. https://doi.org/10.1016/S0967-0637(02)00099-7